ELSEVIER

Comput. Methods Appl. Mech. Engrg. 135 (1996) 107–128

Computer methods in applied mechanics and engineering

Finite element implementation of incompressible, transversely isotropic hyperelasticity

Jeffrey A. Weiss[a,b,*], Bradley N. Maker[c], Sanjay Govindjee[d]

[a]*Applied Mechanics Group, Lawrence Livermore National Laboratory, Livermore, CA 94550, USA*

[b]*Orthopedic Biomechanics Institute, Department of Bioengineering, University of Utah, Salt Lake City, UT 84107, USA*

[c]*Livermore Software Technology Corporation, Livermore, CA 94550, USA*

[d]*Department of Civil Engineering, University of California, Berkeley, Berkeley, CA 94720, USA*

Received 9 June 1995

Abstract

This paper describes a three-dimensional constitutive model for biological soft tissues and its finite element implementation for fully incompressible material behavior. The necessary continuum mechanics background is presented, along with derivations of the stress and elasticity tensors for a transversely isotropic, hyperelastic material. A particular form of the strain energy for biological soft tissues is motivated and a finite element implementation of this model based on a three-field variational principle (deformation, pressure and dilation) is discussed. Numerical examples are presented that demonstrate the utility and effectiveness of this approach for incompressible, transversely isotropic materials.

1. Introduction

The present work was motivated by an interest in the development of computational models of biological joints. Because of the complex nature of joints such as the human knee and shoulder, computational methods are necessary to model their mechanical response. Models of this nature offer the ability to predict soft tissue stresses, joint contact forces and joint kinematics for externally applied loads and displacements. Thus, they promise to offer a general tool for basic and applied research, surgical planning and procedures, teaching and patient education. One of the main hurdles in the development of such models is the availability of finite element implementations of appropriate constitutive models for the soft tissues.

Almost all biological soft tissues are anisotropic, viscoelastic, inhomogeneous, nearly incompressible and undergo large deformations in vivo, both under normal physiological conditions and during injury. Many of these tissues are reinforced by one or more fiber families, usually consisting of collagen and/or elastin. Although the behavior of these tissues is often time- and rate-dependent, they can effectively be modeled by assuming that they are in a 'preconditioned state' in which the behavior may be represented as hyperelastic.

The simplest representation of material anisotropy is transverse isotropy, for which the stress (history) at a material point depends both on the deformation gradient and the 'fiber orientation'. This symmetry class provides an excellent framework for constitutive model development for tissues such as

* Corresponding author.

PII S0045-7825(96)01035-3

ligaments, tendons and cardiac muscle. A considerable amount of research has been directed at the inclusion of this directional dependence into constitutive models of biological soft tissues [3, 10, 11, 13–15, 18, 34], much of which proceeded on an ad hoc basis in an attempt to describe experimentally measured material response.

The objective of this work was to develop an efficient implementation of incompressible hyperelasticity that would accommodate transversely isotropic material symmetry. Section 2 describes the continuum mechanics tools that are necessary to characterize the deformation and the hyperelastic material response. Section 3 presents the formulation of transversely isotropic hyperelasticity in terms of five scalar invariants. The stress and elasticity tensors for an incompressible, transversely isotropic hyperelastic material are presented. Section 4 describes the uncoupling of deviatoric and dilational response in terms of the deformation gradient and the strain energy. Section 5 presents a particular form for the strain energy of a class of transversely isotropic soft tissues that has been motivated by microstructural observations and experimental testing. In Section 6, the finite element formulation based used in this work is described. The formulation is based entirely on the work of Simo et al. [26] and Simo and Taylor [25], who have previously described the three-field variational principle in which displacement, pressure and Jacobian receive separate interpolations. The finite element implementation of a generalized-displacement version of the variational formulation is outlined, along with the implementational specifics. The augmented Lagrangian method is used to enforce fully incompressible behavior. Section 7 provides several numerical examples that demonstrate the accuracy and efficiency of the formulation for fully incompressible transversely isotropic hyperelasticity.

2. Continuum mechanics preliminaries

For later use the following function spaces are defined:

$$\text{Lin} = \text{space of all linear transformations from } \mathbb{R}^3 \text{ into } \mathbb{R}^3 \tag{2.1}$$

with inner product $\boldsymbol{G}:\boldsymbol{H} = \text{tr}(\boldsymbol{G}\boldsymbol{H}^{\mathrm{T}})$, where tr denotes the trace and $\boldsymbol{H}^{\mathrm{T}}$ is the transpose of $\boldsymbol{H}$. We also define

$$\begin{aligned} \text{Lin}^{+} &= \{\boldsymbol{H} \in \text{Lin} : \det \boldsymbol{H} > 0\}\,, \\ \text{Sym}^{+} &= \{\boldsymbol{H} \in \text{Lin} : \boldsymbol{H} = \boldsymbol{H}^{\mathrm{T}}, \boldsymbol{H} \text{ is positive definite}\}\,, \quad \text{and} \\ \text{Orth}^{+} &= \{\boldsymbol{Q} \in \text{Lin}^{+} : \boldsymbol{Q}^{\mathrm{T}}\boldsymbol{Q} = \mathbf{1}\}\,, \end{aligned} \tag{2.2}$$

where det is the determinant and $\mathbf{1}$ is the rank-2 identity tensor.

Denote by $\boldsymbol{\varphi}(\boldsymbol{X}): \Omega \to \mathbb{R}^3$ the deformation map which is assumed to belong to the space

$$\text{Def} = \{\boldsymbol{\varphi} \in C^1(\Omega, \mathbb{R}^3) : \det \nabla\boldsymbol{\varphi} > 0\}\,. \tag{2.3}$$

Here, $\boldsymbol{X} \in \mathbb{R}^3$ designates the position of a particle in the reference configuration Ω. All tensor quantities are written in Cartesian systems throughout this discussion. Whenever indicial notation is employed, lower-case letters refer to the deformed configuration and upper case to the reference configuration. The deformed and reference configurations are related by

$$\boldsymbol{\varphi}(\boldsymbol{X}) = \boldsymbol{X} + \boldsymbol{u}(\boldsymbol{X}) \tag{2.4}$$

where $\boldsymbol{u}$ is the displacement. Let $\boldsymbol{F}$, the *deformation gradient*, be defined as

$$\boldsymbol{F}(\boldsymbol{X}) := \partial\boldsymbol{\varphi}/\partial\boldsymbol{X}\,. \tag{2.5}$$

Further, let

$$J := \det \boldsymbol{F} = \left(\frac{\rho_0}{\rho}\right) \tag{2.6}$$

be the Jacobian of the deformation. For a volume-preserving deformation, $J = 1$. The *right* and *left Cauchy–Green deformation* tensors are, respectively,

$$\boldsymbol{C} := \boldsymbol{F}^{\mathrm{T}}\boldsymbol{F} \quad \text{and} \quad \boldsymbol{B} := \boldsymbol{F}\boldsymbol{F}^{\mathrm{T}} . \tag{2.7}$$

2.1. Hyperelasticity

A general working definition for a *grade 1 elastic material* is that the stress at a point $\boldsymbol{x} = \boldsymbol{\varphi}(\boldsymbol{X})$ is only a function of the deformation gradient $\boldsymbol{F}$ at that point. A change in stress arises solely in response to a change in configuration, and the material is indifferent to the manner in which the change in configuration arises in space and time.

For a *hyperelastic material*, the above definition applies, and in addition there is a scalar function from which the stress can be derived at each point $\boldsymbol{X}$. The scalar function is the stored energy or *strain energy function* $\hat{W} : \Omega \times \mathrm{Lin}^{+} \to \mathbb{R}$. The strain energy, $\hat{W}$, must obey the *Principal of Material Frame Indifference*, which states that constitutive equations must be invariant under changes of observer frame of reference:

$$\hat{W}(\boldsymbol{X}, \boldsymbol{F}) = \hat{W}(\boldsymbol{X}, \boldsymbol{Q}\boldsymbol{F}) \quad \forall\, (\boldsymbol{Q}, \boldsymbol{F}) \in \mathrm{Orth}^{+} \times \mathrm{Lin}^{+} . \tag{2.8}$$

This is equivalent to the requirement that there is a function $\tilde{W} : \Omega \times \mathrm{Sym}^{+} \to \mathbb{R}$

$$\hat{W}(\boldsymbol{X}, \boldsymbol{F}) = \tilde{W}(\boldsymbol{X}, \boldsymbol{F}^{\mathrm{T}}\boldsymbol{F}) \equiv \tilde{W}(\boldsymbol{X}, \boldsymbol{C}) \quad \forall\, \boldsymbol{C} \in \mathrm{Sym}^{+} . \tag{2.9}$$

Any symmetries the material may possess will restrict the way in which the strain energy depends on $\boldsymbol{C}$. Specifically, any orthogonal transformation that is a member of the material symmetry group will leave its strain energy unaltered when applied to the material prior to deformation. For instance, if the material under consideration is *isotropic*, its symmetry group consists of the entire group of proper orthogonal transformations $\boldsymbol{Q}$. In this case, the strain energy can be expressed in the form

$$\hat{W}(\boldsymbol{X}, \boldsymbol{F}) = \hat{W}(\boldsymbol{X}, \boldsymbol{F}\boldsymbol{Q}) \quad \forall\, (\boldsymbol{Q}, \boldsymbol{F}) \in \mathrm{Orth}^{+} \times \mathrm{Lin}^{+} . \tag{2.10}$$

Or, if the Principal of Material Frame Indifference has already been satisfied, then the strain energy function

$$\tilde{W}(\boldsymbol{X}, \boldsymbol{C}) = \tilde{W}(\boldsymbol{X}, \boldsymbol{Q}\boldsymbol{C}\boldsymbol{Q}^{\mathrm{T}}) \qquad \forall\, (\boldsymbol{Q}, \boldsymbol{C}) \in \mathrm{Orth}^{+} \times \mathrm{Sym}^{+} . \tag{2.11}$$

For a material with a particular symmetry group, the task is to determine exactly how the restriction imposed by the symmetry affects the dependence of the strain energy on the deformation gradient.

3. Transverse isotropy

There are two approaches to introducing the directional dependence on the deformation into the strain energy: restrict the way in which the strain energy can depend on the deformation [9], or introduce a vector representing the material preferred direction explicitly into the strain energy [28]. In the former approach, the strain energy can be expressed as a function of the Lagrangian strain components in a coordinate system aligned with the fiber direction. Thus, all computations must be performed in this local coordinate system. In the presentation that follows, we choose the second approach.

We introduce a unit vector field $\boldsymbol{a}^{0}$ in the undeformed configuration that describes the local fiber direction, and require that the strain energy depend on this vector. In this case, the strain energy can be expressed as a function of the right Cauchy–Green deformation tensor and the vector field defining the preferred direction. Further, the strain energy now becomes an isotropic function in both arguments. Smith and Rivlin [27] developed a representation theorem for this case and Spencer [28] has presented relations for the strain energy at a material point in terms of five scalar quantities (invariants) derived from the tensor and vector fields. In the field of biomechanics, this type of representation has been used to model the material behavior of cardiac muscle [13, 14].

When the material undergoes deformation, the vector field $\boldsymbol{a}^{0}(\boldsymbol{X})$ will deform with the body. After deformation the fiber direction may be described by a unit vector field $\boldsymbol{a}(\boldsymbol{\varphi}(\boldsymbol{X}))$. In general, the fibers

will also undergo length change. The fiber stretch, λ, can be determined in terms of the deformation gradient and the fiber direction in the undeformed configuration,

$$\lambda \boldsymbol{a} = \boldsymbol{F} \cdot \boldsymbol{a}^0 . \tag{3.1}$$

Also, since $\boldsymbol{a}$ is a unit vector,

$$\lambda^2 \boldsymbol{a} \cdot \boldsymbol{a} = \lambda^2 = \boldsymbol{a}^0 \cdot \boldsymbol{F}^{\mathrm{T}} \boldsymbol{F} \cdot \boldsymbol{a}^0 = \boldsymbol{a}^0 \cdot \boldsymbol{C} \cdot \boldsymbol{a}^0 . \tag{3.2}$$

This determines the fiber stretch in terms of the deformation gradient and the fiber direction in the undeformed configuration. A material with the above symmetry is called *transversely isotropic*. If it is hyperelastic as well, the form of $\hat{W}$ in (2.8) must now be such that at a point $\boldsymbol{X}$,

$$\hat{W}(\boldsymbol{X}, \boldsymbol{F}) = \hat{W}(\boldsymbol{X}, \boldsymbol{F}\boldsymbol{Q}) \quad \forall (\boldsymbol{Q}, \boldsymbol{F}) \in \{\mathrm{Orth}^+ \times \mathrm{Lin}^+ : \boldsymbol{Q} \cdot \boldsymbol{a}^0 = \boldsymbol{a}^0\} \tag{3.3}$$

Alternatively, the dependence of the strain energy on $\boldsymbol{a}^0$ can be introduced explicitly into $\hat{W}$. In this case, the strain energy is a function of $\boldsymbol{C}$ and $\boldsymbol{a}^0 \otimes \boldsymbol{a}^0$, where $\otimes$ represents the tensor outer product [28]. The invariance of the strain energy with respect to the material symmetry group is now expressed as

$$\bar{W}(\boldsymbol{X}, \boldsymbol{C}, \boldsymbol{a}^0) = \bar{W}(\boldsymbol{X}, \boldsymbol{Q}\boldsymbol{C}\boldsymbol{Q}^{\mathrm{T}}, \boldsymbol{Q}\boldsymbol{a}^0 \otimes \boldsymbol{a}^0 \boldsymbol{Q}^{\mathrm{T}}) \quad \forall (\boldsymbol{Q}, \boldsymbol{C}) \in \mathrm{Orth}^+ \times \mathrm{Sym}^+ \tag{3.4}$$

$\bar{W}$ is then termed an isotropic function of $\boldsymbol{C}$ and $\boldsymbol{a}^0 \otimes \boldsymbol{a}^0$. Spencer has shown that the following set of invariants [28] can be used to fully define the above relations:

$$I_1 = \mathrm{tr}\, \boldsymbol{C} , \qquad I_2 = \tfrac{1}{2}[(\mathrm{tr}\, \boldsymbol{C})^2 - \mathrm{tr}\, \boldsymbol{C}^2] , \qquad I_3 = \det \boldsymbol{C} = J^2 , \tag{3.5}$$

$$I_4 = \boldsymbol{a}^0 \cdot \boldsymbol{C} \cdot \boldsymbol{a}^0 , \qquad I_5 = \boldsymbol{a}^0 \cdot \boldsymbol{C}^2 \cdot \boldsymbol{a}^0 . \tag{3.6}$$

Here, I_1, I_2 and I_3 are the standard invariants of the right Cauchy–Green deformation tensor and the are the complete set of invariants associated with isotropic material behavior. The invariants I_4 and I_5 arise directly from the anisotropy introduced by the reinforcing fiber family. These invariants represent contributions to the strain energy from the properties of the fibers and their interaction with the other material constituents; I_4, for instance, is the square of the stretch along the fiber direction, as in (3.2). With these invariants in hand, the strain energy can be written in terms of a function $W : \mathbb{R}^+ \times \mathbb{R}^+ \times \mathbb{R}^+ \times \mathbb{R}^+ \times \mathbb{R}^+ \to \mathbb{R}$ such that

$$\bar{W}(\boldsymbol{X}, \boldsymbol{C}, \boldsymbol{a}^0) = W(\boldsymbol{X}, I_1(\boldsymbol{C}), I_2(\boldsymbol{C}), I_3(\boldsymbol{C}), I_4(\boldsymbol{C}, \boldsymbol{a}^0), I_5(\boldsymbol{C}, \boldsymbol{a}^0)) . \tag{3.7}$$

With the form (3.7) chosen for the strain energy, the satisfaction of material frame indifference and the material symmetry restrictions for transverse isotropy are assured. This relation is the starting point for deriving the stress and elasticity tensors and also provides the basis for the constitutive model development in the following sections.

3.1. Stress tensors

Our interest is in developing a robust computational representation of transversely isotropic hyperelasticity for an implicit finite element code. The formulation is based upon a linearization about the current configuration, so we require expressions for both the Cauchy stress and spatial version of the 2nd elasticity tensor. This and the following section provide explicit expressions for these tensors in a form suitable for numerical implementation of the corresponding constitutive behavior.

For brevity, the explicit dependence of W on $\boldsymbol{X}$, $\boldsymbol{C}$ and $\boldsymbol{a}^0$ will be omitted in the following discussion. For a hyperelastic material, the 2nd Piola–Kirchhoff stress is derived from the strain energy as

$$\boldsymbol{S} = 2 \frac{\partial W}{\partial \boldsymbol{C}} . \tag{3.8}$$

Using (3.7) and (3.8), we can express $\boldsymbol{S}$ as

$$\boldsymbol{S} = 2\sum_{\alpha=1}^{5}\left(\frac{\partial W}{\partial I_\alpha}\frac{\partial I_\alpha}{\partial \boldsymbol{C}}\right). \tag{3.9}$$

The terms $\partial I_\alpha/\partial \boldsymbol{C}$ can be computed from (3.5) and (3.6):

$$\frac{\partial I_1}{\partial \boldsymbol{C}} = \mathbf{1}, \qquad \frac{\partial I_2}{\partial \boldsymbol{C}} = I_1\mathbf{1} - \boldsymbol{C}, \qquad \frac{\partial I_3}{\partial \boldsymbol{C}} = I_2\mathbf{1} - I_1\boldsymbol{C} + \boldsymbol{C}^2 = I_3\boldsymbol{C}^{-1}, \tag{3.10}$$

$$\frac{\partial I_4}{\partial \boldsymbol{C}} = \boldsymbol{a}^0\otimes\boldsymbol{a}^0, \qquad \frac{\partial I_5}{\partial \boldsymbol{C}} = \boldsymbol{a}^0\otimes\boldsymbol{C}\cdot\boldsymbol{a}^0 + \boldsymbol{a}^0\cdot\boldsymbol{C}\otimes\boldsymbol{a}^0, \tag{3.11}$$

where the reader is reminded that $\mathbf{1}$ represents the rank-2 identity tensor.

If the material is *incompressible*, $I_3 = J^2 = 1$, W is a function of only I_1, I_2, I_4 and I_5; however, an unknown pressure p enters the stress as a reaction to the kinematic constraint on the deformation field. In this case, the 2nd Piola–Kirchhoff stress for an incompressible, transversely isotropic hyperelastic material can be written as

$$\boldsymbol{S} = 2\{(W_1 + I_1W_2)\mathbf{1} - W_2\boldsymbol{C} + W_4\boldsymbol{a}^0\otimes\boldsymbol{a}^0 + W_5(\boldsymbol{a}^0\otimes\boldsymbol{C}\cdot\boldsymbol{a}^0 + \boldsymbol{a}^0\cdot\boldsymbol{C}\otimes\boldsymbol{a}^0)\} + p\boldsymbol{C}^{-1}. \tag{3.12}$$

The Cauchy stress is the push-forward of $\boldsymbol{S}$ by the deformation $\boldsymbol{\varphi}$ [20]:

$$\boldsymbol{\sigma} = \frac{1}{J}\boldsymbol{\varphi}_*(\boldsymbol{S}) \quad\Leftrightarrow\quad (\boldsymbol{\sigma})_{ij} = \frac{1}{J}F_{iI}F_{jJ}S_{IJ} \tag{3.13}$$

$$= 2\{(W_1 + I_1W_2)\boldsymbol{B} - W_2\boldsymbol{B}^2 + I_4W_4\boldsymbol{a}\otimes\boldsymbol{a} + I_4W_5(\boldsymbol{a}\otimes\boldsymbol{B}\cdot\boldsymbol{a} + \boldsymbol{a}\cdot\boldsymbol{B}\otimes\boldsymbol{a})\} + p\mathbf{1}. \tag{3.14}$$

Here, the notation $W_a = \partial W/\partial I_a$ has been introduced. Note that both $\boldsymbol{S}$ and $\boldsymbol{\sigma}$ are symmetric. The above results are due to Spencer [28].

3.2. Elasticity tensors

The material version of the 2nd elasticity tensor is defined as

$$\mathbf{C} := 4\frac{\partial^2 W}{\partial \boldsymbol{C}\,\partial \boldsymbol{C}} = 2\frac{\partial \boldsymbol{S}}{\partial \boldsymbol{C}}. \tag{3.15}$$

To determine the form of $\mathbf{C}$, we first note the following relations

$$\frac{\partial C_{IJ}}{\partial C_{KL}} = \frac{1}{2}(\delta_{IK}\,\delta_{JL} + \delta_{IL}\,\delta_{JK}) := I_{IJKL}, \tag{3.16}$$

and

$$\frac{\partial C^{-1}_{IJ}}{\partial C_{KL}} = -\frac{1}{2}(C^{-1}_{IK}C^{-1}_{JL} + C^{-1}_{IL}C^{-1}_{JK}) := (I_{C^{-1}})_{IJKL}. \tag{3.17}$$

Using (3.15) and (3.12) with the product and chain rules, the material elasticity tensor takes the form

$$\begin{aligned}\mathbf{C} = 4\Big\{&\mathbf{1}\otimes\frac{\partial W_1}{\partial \boldsymbol{C}} + \mathbf{1}\otimes W_2\frac{\partial I_1}{\partial \boldsymbol{C}} + \mathbf{1}\otimes I_1\frac{\partial W_2}{\partial \boldsymbol{C}} - \boldsymbol{C}\otimes\frac{\partial W_2}{\partial \boldsymbol{C}} - W_2\frac{\partial \boldsymbol{C}}{\partial \boldsymbol{C}}\\ &+ \boldsymbol{a}^0\otimes\boldsymbol{a}^0\otimes\frac{\partial W_4}{\partial \boldsymbol{C}} + \frac{\partial I_5}{\partial \boldsymbol{C}}\otimes\frac{\partial W_5}{\partial \boldsymbol{C}} + W_5\frac{\partial^2 I_5}{\partial \boldsymbol{C}\,\partial \boldsymbol{C}}\Big\} + p\boldsymbol{I}_{C^{-1}}\end{aligned} \tag{3.18}$$

After further application of the chain rule to the terms $\partial W_a/\partial \boldsymbol{C}$ and some manipulation, the material elasticity tensor for an incompressible, transversely isotropic, hyperelastic material takes the form

$$\begin{aligned}\mathbf{C} = 4\Big\{&(W_{11} + 2W_{12}I_1 + W_2 + W_{22}I_1^2)\mathbf{1}\otimes\mathbf{1}\\ &- (W_{12} + W_{22}I_1)(\mathbf{1}\otimes\boldsymbol{C} + \boldsymbol{C}\otimes\mathbf{1}) + W_{22}(\boldsymbol{C}\otimes\boldsymbol{C}) - W_2\boldsymbol{I}\\ &+ (W_{14} + W_{24}I_1)(\mathbf{1}\otimes\boldsymbol{a}^0\otimes\boldsymbol{a}^0 + \boldsymbol{a}^0\otimes\boldsymbol{a}^0\otimes\mathbf{1}) + W_5\frac{\partial^2 T_5}{\partial \boldsymbol{C}\,\partial \boldsymbol{C}}\end{aligned}$$

$$
\begin{aligned}
&+ (W_{15} + W_{25} I_1)\left(\mathbf{1} \otimes \frac{\partial I_5}{\partial \boldsymbol{C}} + \frac{\partial I_5}{\partial \boldsymbol{C}} \otimes \mathbf{1}\right) \\
&- W_{24}(\boldsymbol{C} \otimes \boldsymbol{a}^0 \otimes \boldsymbol{a}^0 + \boldsymbol{a}^0 \otimes \boldsymbol{a}^0 \otimes \boldsymbol{C}) - W_{25}\left(\boldsymbol{C} \otimes \frac{\partial I_5}{\partial \boldsymbol{C}} + \frac{\partial I_5}{\partial \boldsymbol{C}} \otimes \boldsymbol{C}\right) \\
&+ W_{44}(\boldsymbol{a}^0 \otimes \boldsymbol{a}^0 \otimes \boldsymbol{a}^0 \otimes \boldsymbol{a}^0) + W_{45}\left(\boldsymbol{a}^0 \otimes \boldsymbol{a}^0 \otimes \frac{\partial I_5}{\partial \boldsymbol{C}} + \frac{\partial I_5}{\partial \boldsymbol{C}} \otimes \boldsymbol{a}^0 \otimes \boldsymbol{a}^0\right) \\
&+ W_{55}\left(\frac{\partial I_5}{\partial \boldsymbol{C}} \otimes \frac{\partial I_5}{\partial \boldsymbol{C}}\right)\Big\} + p \boldsymbol{I}_{C^{-1}} \,. \qquad (3.19)
\end{aligned}
$$

Where the notation $W_{ab} = \partial^2 W / \partial I_a \, \partial I_b$ has been introduced. Note also that $\mathbf{C}$ possesses both major and minor symmetries. The spatial version of the 2nd elasticity tensor is defined as the push-forward of $\mathbf{C}$ by the deformation $\boldsymbol{\varphi}$,

$$
\mathbf{c} := \frac{1}{J} \boldsymbol{\varphi}_*(\mathbf{C}) \quad \Leftrightarrow \quad c_{ijkl} = \frac{1}{J} F_{iI} F_{jJ} F_{kK} F_{lL} C_{IJKL} \,, \qquad (3.20)
$$

Using (3.20), one arrives at

$$
\begin{aligned}
\mathbf{c} = 4\Big\{&(W_{11} + 2W_{12} I_1 + W_2 + W_{22} I_1^2) \boldsymbol{B} \otimes \boldsymbol{B} \\
&- (W_{12} + W_{22} I_1)(\boldsymbol{B} \otimes \boldsymbol{B}^2 + \boldsymbol{B}^2 \otimes \boldsymbol{B}) + W_{22}(\boldsymbol{B}^2 \otimes \boldsymbol{B}^2) - W_2 \boldsymbol{I}_{B^{-1}} \\
&+ (W_{14} + W_{24} I_1) I_4 (\boldsymbol{B} \otimes \boldsymbol{a} \otimes \boldsymbol{a} + \boldsymbol{a} \otimes \boldsymbol{a} \otimes \boldsymbol{B}) + W_5 \boldsymbol{\varphi}_* \frac{\partial^2 I_5}{\partial \boldsymbol{C} \, \partial \boldsymbol{C}} \\
&+ (W_{15} + W_{25} I_1)\left(\boldsymbol{B} \otimes \left[\boldsymbol{\varphi}_* \frac{\partial I_5}{\partial \boldsymbol{C}}\right] + \left[\boldsymbol{\varphi}_* \frac{\partial I_5}{\partial \boldsymbol{C}}\right] \otimes \boldsymbol{B}\right) \\
&- W_{24} I_4^2 (\boldsymbol{B} \otimes \boldsymbol{a} \otimes \boldsymbol{a} + \boldsymbol{a} \otimes \boldsymbol{a} \otimes \boldsymbol{B}^2) - W_{25}\left(\boldsymbol{B}^2 \otimes \left[\boldsymbol{\varphi}_* \frac{\partial I_5}{\partial \boldsymbol{C}}\right] + \left[\boldsymbol{\varphi}_* \frac{\partial I_5}{\partial \boldsymbol{C}}\right] \otimes \boldsymbol{B}^2\right) \\
&+ W_{44} I_4^2 (\boldsymbol{a} \otimes \boldsymbol{a} \otimes \boldsymbol{a} \otimes \boldsymbol{a}) + W_{45} I_4 \left(\boldsymbol{a} \otimes \boldsymbol{a} \otimes \left[\boldsymbol{\varphi}_* \frac{\partial I_5}{\partial \boldsymbol{C}}\right] + \left[\boldsymbol{\varphi}_* \frac{\partial I_5}{\partial \boldsymbol{C}}\right] \otimes \boldsymbol{a} \otimes \boldsymbol{a}\right) \\
&+ W_{55}\left(\left[\boldsymbol{\varphi}_* \frac{\partial I_5}{\partial \boldsymbol{C}}\right] \otimes \left[\boldsymbol{\varphi}_* \frac{\partial I_5}{\partial \boldsymbol{C}}\right]\right)\Big\} + p \boldsymbol{I} \,, \qquad (3.21)
\end{aligned}
$$

where

$$
(\boldsymbol{\varphi}_* \boldsymbol{I})_{ijkl} = -\tfrac{1}{2}(B^{-1}_{ik} B^{-1}_{jl} + B^{-1}_{il} B^{-1}_{jk}) := (I_{B^{-1}})_{ijkl} \,, \qquad (3.22)
$$

and

$$
\boldsymbol{\varphi}_* \frac{\partial I_5}{\partial \boldsymbol{C}} = I_4 (\boldsymbol{a} \otimes \boldsymbol{B} \cdot \boldsymbol{a} + \boldsymbol{a} \cdot \boldsymbol{B} \otimes \boldsymbol{a}) \,. \qquad (3.23)
$$

These closed-form expressions for $\mathbf{C}$ and $\mathbf{c}$ do not appear to have been reported previously in the literature.

4. Uncoupling of deviatoric and dilational response

It is well known that displacement-based finite element methods are difficult to use in the analysis of nearly incompressible materials. These difficulties include numerical ill-conditioning of the stiffness matrix due to the larger contributions from the dilational stiffness on the diagonal, spurious, or incorrect pressures and 'locking' of the mesh due to overconstraint of the displacement field (see e.g. [12, 17, 23, 39]). In anticipation of these difficulties, we will apply separate numerical treatment to the dilational and deviatoric parts of the deformation gradient.

4.1. Multiplicative split of deformation gradient

To decouple deviatoric and dilational response, the following multiplicative decomposition is introduced [4]:

$$\boldsymbol{F} = \boldsymbol{F}_{\text{vol}}\tilde{\boldsymbol{F}}\,, \qquad \boldsymbol{F}_{\text{vol}} := J^{1/3}\mathbf{1} \quad \text{and} \quad \tilde{\boldsymbol{F}} := J^{-1/3}\boldsymbol{F}\,. \tag{4.1}$$

Clearly, by construction

$$\det \boldsymbol{F}_{\text{vol}} = J \quad \text{and} \quad \det \tilde{\boldsymbol{F}} = 1 \tag{4.2}$$

so that only the deformation due to $\boldsymbol{F}_{\text{vol}}$ contributes to the volume change of the material. The total dependence of a function on the deformation gradient can be expressed in terms of $\tilde{\boldsymbol{F}}$, J and their interaction. Similarly, the right Cauchy–Green deformation tensor is decomposed as

$$\boldsymbol{C} = \boldsymbol{F}^{\mathrm{T}}\boldsymbol{F} = J^{2/3}\tilde{\boldsymbol{C}}\,, \quad \text{where} \quad \tilde{\boldsymbol{C}} = \tilde{\boldsymbol{F}}^{\mathrm{T}}\tilde{\boldsymbol{F}}\,. \tag{4.3}$$

4.2. Uncoupled strain energy

Following the approach taken by others in the representation of quasi-incompressible elasticity [26], it is assumed that the strain energy function for a slightly compressible material takes an uncoupled form, in which the dilational and deviatoric components are such that

$$W = U(J) + \tilde{W}(\tilde{\boldsymbol{C}})\,. \tag{4.4}$$

(The use of $\tilde{W}$ here is not to be confused with the $\tilde{W}$ of Section 2.2.) This assumption is based more on mathematical convenience rather than physical observations – it allows the second elasticity tensors and thus the resulting tangent stiffness from a three-field variational principle to be expressed in a much reduced from. Also, the decoupling of the pressure variable from the stress is now trivial.

With the form (4.4) chosen for the strain energy, the stress can be written as

$$\boldsymbol{S} = pJ\boldsymbol{C}^{-1} + 2J^{-2/3}\,\mathrm{DEV}\left[\frac{\partial \tilde{W}}{\partial \tilde{\boldsymbol{C}}}\right]. \tag{4.5}$$

The identification $U'(J) = p$, where p is the hydrostatic pressure, has been made. Note that for the uncoupled strain energy, p also represents the total dilational stress. The operator DEV[·] is the deviatoric projection operator for stress-like quantities in the reference configuration:

$$\mathrm{DEV}[\cdot] \equiv [\cdot] - \tfrac{1}{3}([\cdot]:\tilde{\boldsymbol{C}})\tilde{\boldsymbol{C}}^{-1}\,. \tag{4.6}$$

By computing the push-forward of (4.5), the Cauchy stress is

$$\boldsymbol{\sigma} = p\mathbf{1} + \frac{2}{J}\,\mathrm{dev}\left[\tilde{\boldsymbol{F}}\,\frac{\partial \tilde{W}}{\partial \tilde{\boldsymbol{C}}}\,\tilde{\boldsymbol{F}}^{\mathrm{T}}\right] \tag{4.7}$$

where

$$\mathrm{dev}[\cdot] \equiv [\cdot] - \tfrac{1}{3}([\cdot]:\mathbf{1})\mathbf{1}\,. \tag{4.8}$$

The explicit expression for the material elasticity tensor, $\mathbf{C}$, follows from (3.15):

$$\begin{aligned}\mathbf{C} = {} & pJ(\boldsymbol{C}^{-1}\otimes\boldsymbol{C}^{-1} - 2\boldsymbol{I}_{C^{-1}}) - \frac{4}{3}J^{4/3}\left(\frac{\partial \tilde{W}}{\partial \tilde{\boldsymbol{C}}}\otimes\tilde{\boldsymbol{C}}^{-1} + \tilde{\boldsymbol{C}}^{-1}\otimes\frac{\partial \tilde{W}}{\partial \tilde{\boldsymbol{C}}}\right) \\ & + \frac{4}{3}J^{4/3}\left(\frac{\partial \tilde{W}}{\partial \tilde{\boldsymbol{C}}}:\tilde{\boldsymbol{C}}\right)(\boldsymbol{I}_{C^{-1}} + \frac{1}{3}\tilde{\boldsymbol{C}}^{-1}\otimes\tilde{\boldsymbol{C}}^{-1}) + J^{4/3}\tilde{\mathbf{C}}_{\tilde{W}}\,,\end{aligned} \tag{4.9}$$

where $\tilde{\mathbf{C}}_{\tilde{W}}$ is the portion of $\mathbf{C}$ arising directly from second derivatives of $\tilde{W}$ with respect to $\tilde{\boldsymbol{C}}$. It is defined as

$$\tilde{\mathbf{C}}_{\tilde{W}} = 4\frac{\partial^2 \tilde{W}}{\partial \tilde{\boldsymbol{C}}\,\partial \tilde{\boldsymbol{C}}} - \frac{4}{3}\left[\left(\frac{\partial^2 \tilde{W}}{\partial \tilde{\boldsymbol{C}}\,\partial \tilde{\boldsymbol{C}}} : \tilde{\boldsymbol{C}}\right) \otimes \tilde{\boldsymbol{C}}^{-1} + \tilde{\boldsymbol{C}}^{-1} \otimes \left(\frac{\partial^2 \tilde{W}}{\partial \tilde{\boldsymbol{C}}\,\partial \tilde{\boldsymbol{C}}} : \tilde{\boldsymbol{C}}\right)\right] + \frac{4}{9}\left(\tilde{\boldsymbol{C}} : \frac{\partial^2 \tilde{W}}{\partial \tilde{\boldsymbol{C}}\,\partial \tilde{\boldsymbol{C}}} : \tilde{\boldsymbol{C}}\right)\tilde{\boldsymbol{C}}^{-1} \otimes \tilde{\boldsymbol{C}}^{-1}. \tag{4.10}$$

These relations would be considerably more complicated if the strain energy were coupled – then there would be terms of the form $\partial/\partial \boldsymbol{C}$ $(\partial W/\partial \tilde{\boldsymbol{C}}\ \partial \tilde{\boldsymbol{C}}/\partial \boldsymbol{C})$. Now, the push forward relation (3.20) can be used to obtain the spatial elasticity tensor. Noting the identity $F^i_I F^j_J F^k_K F^l_L I^{IJKL}_{C^{-1}} = I^{ijkl}$,

$$\mathbf{c} = p(\mathbf{1}\otimes\mathbf{1} - 2\boldsymbol{I}) - \frac{2}{3}(\operatorname{dev}\boldsymbol{\sigma}\otimes\mathbf{1} + \mathbf{1}\otimes\operatorname{dev}\boldsymbol{\sigma}) + \frac{4}{3J}\left(\frac{\partial \tilde{W}}{\partial \tilde{\boldsymbol{C}}} : \tilde{\boldsymbol{C}}\right)\left[\boldsymbol{I} - \frac{1}{3}(\mathbf{1}\otimes\mathbf{1})\right] + \tilde{\mathbf{c}}_{\tilde{W}}, \tag{4.11}$$

where $\tilde{\mathbf{c}}_{\tilde{W}}$ is the push-forward of $\tilde{\mathbf{C}}_{\tilde{W}}$:

$$\tilde{c}^{ijkl}_{\tilde{W}} = \frac{1}{J}\tilde{F}^i_I \tilde{F}^j_J \tilde{F}^k_K \tilde{F}^l_L \tilde{C}^{IJKL}_{\tilde{W}}. \tag{4.12}$$

These expressions for the uncoupled stress and elasticity tensors are apparently due to Simo et al. [26]

5. A particular W for biological soft tissues

Biological soft tissues are anisotropic, viscoelastic, inhomogeneous and undergo large deformations. However, the constitutive behavior of many soft tissues is relatively insensitive to strain rate over several decades of variation [7]. Also, these tissues reach a 'preconditioned' state after repeated loadings; the loading and unloading cycles of the material are then repeatable and there is a minimal amount of hysteresis (Fig. 1). There is also a minimal amount of relaxation/creep and the peak stress during cyclic loading no longer decreases with time. These 'pseudoelastic' tissues can then be modeled using a hyperelastic approach. Hyperelasticity provides an ideal framework for numerical modeling of pseudoelastic soft tissue structures because it allows for large deformations and anisotropy. With a finite element approach, inhomogeneities can be modeled if data are available. These models can be easily modified to extend their applicability to viscoelasticity and damage mechanics [8, 24].

Many soft tissues, such as ligaments and tendons, are composed mainly of collagen fibers that run parallel to the predominant axis of loading in vivo. These tissues also contain elastin, proteoglycans, glycolipids, water and fibroblasts (cells) [33]. All the tissue components together, except the collagen,

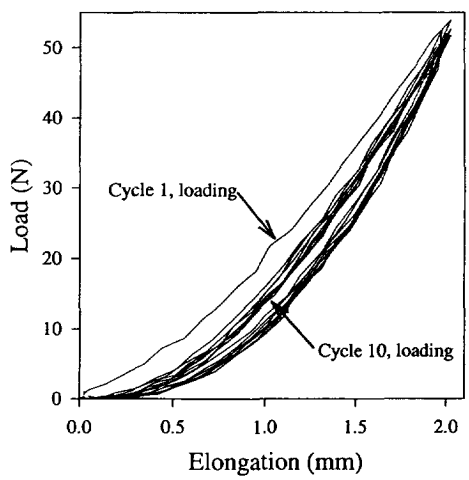

Fig. 1. Cyclic load-elongation behavior of human fascia lata tested along the fiber direction. The hysteresis decreases with increasing cycle number, and the loading-unloading curves become repeatable [31].

are referred to as the ground substance matrix. The water comprises between 60 and 70% of the total weight of tissues such as ligaments and tendons, but it appears to be tightly bound to the matrix as it is difficult exude any significant amount under compressive pressure [16]. The microstructural organization of the constituents in these soft tissues yields mechanical characteristics that are crucial to physiological function. The overall response of the tissue to applied loads and/or deformation is directly a result of the mechanical response of and interaction between its constituent materials.

5.1. *A form for the strain energy*

For the purposes of this model, the elastic response of the tissue will be assumed to arise from the resistance of the collagen fiber family, the ground substance matrix, and their interaction. Further, it is assumed that the collagen fibers are responsible for the transversely isotropic symmetry and that the ground substance, or matrix, is isotropic. Within the framework of incompressible, transversely isotropic hyperelasticity, the strain energy can then be written as

$$W = F_1(I_1, I_2) + F_2(I_4) + F_3(I_1, I_2, I_4) \tag{5.1}$$

where I_1 and I_2 are the invariants of the right Cauchy–Green deformation tensor described by (3.5) and I_4 is given by (3.6). The function F_1 represents the material response of the isotropic ground substance matrix, F_2 represents the contribution from the collagen fiber family, and F_3 is the contribution from interactions between the fibers and matrix.

The dependence of W on I_4, as suggested by (3.7), can easily be replaced by an equivalent dependence on the stretch along the fiber direction, λ. This makes it somewhat easier to fit experimental data to the function. The dependence on I_3 has been omitted because of the incompressibility constraint ($J = \sqrt{I_3} = 1$). The dependence on I_5 has been omitted as well, as many of the effects governed by I_5 can be introduced into the function through the derivatives of the strain energy with respect to I_4.

The form (5.1) generalizes many constitutive equations that have been successfully used in the past to describe biological soft tissues (e.g. [3, 11, 13, 14]). While this relation represents a large simplification when compared to the general case, it also embodies almost all of the material behavior that one would expect from transversely isotropic, large-deformation matrix-fiber composites.

The Mooney–Rivlin material [22] offers an example of a form that can be used to describe the ground substance matrix:

$$F_1 = \frac{C_1}{2}(I_1 - 3) + \frac{C_2}{2}(I_2 - 3)\,, \tag{5.2}$$

where the constants C_1 and C_2 are to be determined from experimental tests. If the constant C_2 is zero, then the resulting model is the neo-Hookean material. For many biological soft tissues, an exponential function may be appropriate for F_2 [6].

The function F_3 controls the interaction between the collagen fiber family and the ground substance matrix. This can take several forms. Stretch along the fiber direction could cause stress to develop in the matrix, or vice versa. It is more likely that such an interaction would take the form of a shear coupling. Because shear testing is required to determine such effects, the experimental aspects are difficult. The applicability of (5.1) to the modeling of ligaments and tendons has been determined by experiment [31].

The uncoupled versions of the stress and elasticity tensors corresponding to (5.1) are presented in the Appendix.

6. Finite element implementation

The proper treatment of incompressible material response is essential to the modeling of biological soft tissues. Because this assumption is often made during materials testing and in the formulation of constitutive models, it must be satisfied by the numerical solutions as well. Failure to satisfy the constraint can result in considerable drift of the numerical solution from the theoretical solution.

6.1. Three-field variational principle

The previously developed equations for an uncoupled strain energy are used to describe a variational principle that yields an efficient finite element formulation for quasi- and fully-incompressible hyperelastic materials. This variational principle incorporates the configuration $\boldsymbol{\varphi}$, dilation Θ and pressure p as field variables as proposed in [26]. Introductory discussions and original references on three field variational principles can be found in [5, Section 16.7], [30, Section 3.9]. This approach provides several advantages when used to develop finite element approximations: 1) the interpolated pressure is the total hydrostatic stress, 2) the interpolated volume ratio can be constrained to unity (or some other value) by an augmented Lagrangian method, and 3) it provides a variational framework for mixed penalty methods, assumed strain methods, and selective integration schemes.

Following from [25], a variational principle must be constructed that contains all three field variables. A *modified* deformation gradient $\bar{\boldsymbol{F}}$, is constructed which depends on both $\boldsymbol{\varphi}$ and Θ,

$$\bar{\boldsymbol{F}} := \Theta^{1/3}\tilde{\boldsymbol{F}} \equiv \Theta^{1/3}[J(\boldsymbol{\varphi})]^{-1/3}\frac{\partial \boldsymbol{\varphi}}{\partial \boldsymbol{X}}, \tag{6.1}$$

where $J(\boldsymbol{\varphi}) := \det[\partial \boldsymbol{\varphi}/\partial \boldsymbol{X}]$. The corresponding right Cauchy–Green deformation tensor $\bar{\boldsymbol{C}}$ is then

$$\bar{\boldsymbol{C}}(\boldsymbol{\varphi}, \Theta) := [\bar{\boldsymbol{F}}(\boldsymbol{\varphi}, \Theta)]^{\mathrm{T}}\bar{\boldsymbol{F}}(\boldsymbol{\varphi}, \Theta). \tag{6.2}$$

Now a functional Π is defined in terms of $\boldsymbol{\varphi}$, Θ and p,

$$\Pi(\boldsymbol{\varphi}, \Theta, p) := \int_{\Omega} \{W(\boldsymbol{X}, \bar{\boldsymbol{C}}(\boldsymbol{\varphi}, \Theta)) + p(J(\boldsymbol{\varphi}) - \Theta)\}\, \mathrm{d}V + \Pi_{\mathrm{ext}}(\boldsymbol{\varphi}), \tag{6.3}$$

where Π_{ext} is the potential energy of the external loading in the reference configuration. By setting the first variation of Π with respect to the field variables $(\boldsymbol{\varphi}, \Theta, p)$ in the arbitrary directions $(\boldsymbol{\eta}, \psi, q)$ equal to zero, we obtain the Euler–Lagrange equations:

$$\begin{aligned} D_{\varphi}\Pi \cdot \boldsymbol{\eta} &= \int_{\varphi(\Omega)} (\mathrm{dev}[\boldsymbol{\sigma}] : \mathrm{dev}[\nabla \boldsymbol{\eta}] + p\ \mathrm{div}\ \boldsymbol{\eta})\, \mathrm{d}v - g_{\mathrm{ext}}(\boldsymbol{\eta}) = 0, \\ D_{\Theta}\Pi \cdot \psi &= \int_{\varphi(\Omega)} \psi\left\{\frac{1}{3\Theta}\,\mathrm{tr}[\boldsymbol{\sigma}] - p\right\} \mathrm{d}v/J = 0, \\ D_{p}\Pi \cdot q &= \int_{\varphi(\Omega)} q\{J - \Theta\}\, \mathrm{d}v/J = 0, \end{aligned} \tag{6.4}$$

where $g_{\mathrm{ext}}(\boldsymbol{\eta})$ is the virtual work of the external loading in the spatial description. The first equation implies that external loads must balance with the internal stresses. The second equation implies that the dilational stress is equal to the hydrostatic pressure (a result of the uncoupled strain energy function). The third equation implies that Θ will equal J (the Jacobian determined from the displacement field) at equilibrium. The incompressibility constraint has not yet been enforced.

6.2. Mixed finite element formulation

We introduce a finite element approximation for the pressure and dilation, by *discontinuous* local interpolation over the *current* element configuration $\boldsymbol{\varphi}(\Omega_e)$ on a typical element Ω_e. The interpolations over an element for dilation and pressure are then

$$\Theta_e \equiv \Theta|_{\varphi(\Omega_e)} = \sum_{k=1}^{\bar{N}} \Psi_k(\boldsymbol{X})\Theta_k, \tag{6.5}$$

$$p_e \equiv p|_{\varphi(\Omega_e)} = \sum_{k=1}^{\bar{N}} \Psi_k(\boldsymbol{X})p_k, \tag{6.6}$$

for the $\bar{N}$ polynomials $\boldsymbol{\Psi}(\boldsymbol{X})$. Θ_k and p_k are nodal values of the dilation and pressure, respectively. The subscript e emphasizes the restriction to a particular element. An isoparametric conforming finite element approximation of the space of admissible variations is defined in the standard manner as

$$\boldsymbol{\eta}_e \equiv \boldsymbol{\eta}|_{\varphi(\Omega_e)} = \sum_{k=1}^{N_{\text{nodes}}} N_k(\boldsymbol{\xi})\boldsymbol{\eta}_k\,, \quad \boldsymbol{\eta}_k \in \mathbb{R}^3\,. \tag{6.7}$$

Here, $\boldsymbol{\xi} \in \square$, where $\square := \{(-1,1)\times(-1,1)\times(-1,1)\}$ is the bi-unit cube, N_k the isoparametric shape functions, and

$$\boldsymbol{X}_e = \sum_{k=1}^{N_{\text{nodes}}} N_k(\boldsymbol{\xi})\boldsymbol{X}_k \tag{6.8}$$

is the isoparametric map. The deformed configuration of an element is then computed using the shape functions as

$$\boldsymbol{\varphi}_e = \boldsymbol{X}_e + \boldsymbol{U}_e = \sum_{k=1}^{N_{\text{nodes}}} N_k(\boldsymbol{\xi})(\boldsymbol{X}_k + \boldsymbol{U}_k)\,, \tag{6.9}$$

where $\boldsymbol{U}_e$ is the discrete displacement field restricted to Ω_e.

6.3. Generalized displacement model

For speed of computation, a trilinear interpolation is used for the displacement fields, and the dilation and pressure are assumed constant on an element. Then the shape function for the dilation and pressure is simply

$$\Psi = 1\,. \tag{6.10}$$

Then, Θ_e is the average Jacobian over the element,

$$\Theta_e = \frac{\int_\square J_e j_\xi \,\mathrm{d}\boldsymbol{\xi}}{\int_\square j_\xi \,\mathrm{d}\boldsymbol{\xi}} \equiv \frac{V_e}{V_e^0}\,, \tag{6.11}$$

where j_ξ is the Jacobian of the isoparametric map,

$$j_\xi = \det\left[\sum_{k=1}^{N_{\text{nodes}}} \frac{\partial N_k}{\partial \boldsymbol{\xi}} \boldsymbol{X}_k\right]. \tag{6.12}$$

V_e and V_e^0 are the volume of the element in the deformed and undeformed configurations, respectively. The pressure is also computed easily as

$$p_e = \frac{1}{V_e^0}\int_\square U'(\Theta) j_\xi \,\mathrm{d}\boldsymbol{\xi} = U'(\Theta) \tag{6.13}$$

Restricting (6.4) to an individual element and inserting the expressions (6.11) and (6.13), the generalized displacement model is

$$G(\boldsymbol{\varphi}, \boldsymbol{\eta})|_{\Omega_e} = \int_\square [\boldsymbol{\sigma}_e : \nabla^s \boldsymbol{\eta}] J_e j_\xi \,\mathrm{d}\boldsymbol{\xi} - g_{\text{ext}}(\boldsymbol{\eta})|_{\Omega_e} = 0\,. \tag{6.14}$$

Here, $J_e = \det \boldsymbol{F}_e$. The stress is computed on the element level using

$$\boldsymbol{\sigma}_e = p_e + \frac{1}{J_e}\,\mathrm{dev}\left[\tilde{\boldsymbol{F}}_e \frac{\partial \tilde{W}(X, \tilde{\boldsymbol{C}}_e)}{\partial \tilde{\boldsymbol{C}}_e} \tilde{\boldsymbol{F}}_e^{\mathrm{T}}\right]. \tag{6.15}$$

$\boldsymbol{F}_e$ is computed using (6.9), and the (symmetric) gradient operator is computed in terms of the derivatives of the shape functions as

$$\nabla^s \boldsymbol{\eta} = \sum_{k=1}^{N_{\text{nodes}}} \boldsymbol{B}_k \boldsymbol{\eta}_k \tag{6.16}$$

where $\boldsymbol{B}$ is the standard (linear) strain–displacement matrix [2].

6.4. Matrix form of the finite element equations

Assuming that the solution at a configuration $\boldsymbol{\varphi}_0$ is known, we seek the solution at some increment $\boldsymbol{\varphi}_0 + \Delta\boldsymbol{u}$. The starting point is the consistent linearization of the generalized displacement model G_e at $\boldsymbol{\varphi}_0$ to get an initial estimate for $\Delta\boldsymbol{u}$. This estimate for $\Delta\boldsymbol{u}$ is then iteratively improved using a Newton (or quasi-Newton) method. The linearization takes the form:

$$L_{\boldsymbol{\varphi}_0} G_e(\boldsymbol{\varphi}) = G_e(\boldsymbol{\varphi}_0) + DG_e(\boldsymbol{\varphi}_0) \cdot (\Delta\boldsymbol{u}) \,. \tag{6.17}$$

The linearization of (6.14) about a configuration $\boldsymbol{\varphi} = \boldsymbol{\varphi}_0$ yields, on the element level, a system of linear algebraic equations of the form

$$\sum_{i=1}^{N_{\text{nodes}}} \sum_{j=1}^{N_{\text{nodes}}} ({}^{\text{M}}\boldsymbol{K}(\boldsymbol{\varphi}_0) + {}^{\text{G}}\boldsymbol{K}(\boldsymbol{\varphi}_0) + {}^{\text{MIX}}\boldsymbol{K}(\boldsymbol{\varphi}_0))_{ij} \, \Delta\boldsymbol{u} = \sum_{i=1}^{N_{\text{nodes}}} ({}^{\text{ext}}\boldsymbol{F} - {}^{\text{int}}\boldsymbol{F}(\boldsymbol{\varphi}_0))_i \tag{6.18}$$

The term ${}^{\text{M}}\boldsymbol{K}$ represents the material stiffness matrix, while the term ${}^{\text{G}}\boldsymbol{K}$ is the geometric (initial stress) stiffness matrix. These terms both arise in a traditional displacement-based non-linear analysis. The mixed stiffness, ${}^{\text{MIX}}\boldsymbol{K}$, is a direct result of the discontinuous interpolation of p_e and Θ_e and the consistent linearization. $\Delta\boldsymbol{u}$ is the initial guess at the increment to the unknown configuration $\boldsymbol{\varphi}_{n+1}$. By solving for $\Delta\boldsymbol{u}$, the configuration at $n+1$ is approximated as

$$\boldsymbol{\varphi}_{n+1} = \boldsymbol{\varphi}_0 + s \, \Delta\boldsymbol{u} \,. \tag{6.19}$$

Here, s is a scalar parameter between 0 and 1 determined by a line search. The determination of an accurate value for $\boldsymbol{\varphi}_{n+1}$ follows by iterative solution of (6.14) using a Newton (or quasi-Newton) strategy in conjunction with (6.18) [21].

6.5. Augmented Lagrangian method for incompressible response

The previously described finite element formulation avoids the 'locking' behavior that can result for nearly- and full-incompressible response. However, it does not ensure that the material being modeled will behave as incompressible. To enforce the incompressibility constraint without losing the computational advantage of the generalized displacement model, an augmented Lagrangian method is utilized [25]. With augmented Lagrangian methods, the governing equations are first solved with relatively compressible material behavior. Then, a Lagrange multiplier, λ, corresponding to a form of the incompressibility constraint is incrementally determined. With proper update of Θ_e and p_e, this leads to a stable algorithm that allows the incompressibility constraint to be satisfied to any desired tolerance. The ill-conditioning of the tangent stiffness associated with the penalty method is avoided. The variational functional is defined as in (6.3) with the addition of a term that represents the added constraint on Θ due to the augmentation,

$$\mathscr{L}(\boldsymbol{\varphi}, \Theta, p; \lambda) = \Pi(\boldsymbol{\varphi}, \Theta, p) + \int_\Omega \lambda h(\Theta) \, \mathrm{d}V \,, \tag{6.20}$$

where λ is the multiplier. The function $h(\Theta)$ is such that $h(\Theta) = 0$ iff $\Theta = 1$. In the analyses to be discussed, the functions $U(\Theta)$ and $h(\Theta)$ were

$$U(\Theta) = \frac{\varepsilon}{2} \ln(\Theta)^2 \,; \qquad h(\Theta) = \lambda \ln(\Theta) \tag{6.21}$$

where ε is the penalty parameter. For an incompressible material, the functions do not provide any contribution to the pressure or stress. If quasi-incompressible behavior is to be modeled, the function $U(\Theta)$ can be determined from experiment.

7. Numerical examples

The finite element method outlined in the previous section was implemented in the general purpose finite element code NIKE3D, developed and maintained by the Methods Development Group at Lawrence Livermore National Laboratory [19]. The transversely isotropic material model allows for specification of preferred material directions in terms of a global vector or locally based upon an orthogonal system derived from each element's nodal points. The deviatoric strain energy, $\tilde{W}$, is defined in a subroutine in terms of the derivatives with respect to the deviatoric invariants $\tilde{I}_1$, $\tilde{I}_2$ and $\tilde{I}_4$. The dilational strain energy, $U(\Theta)$, and the augmented Lagrangian function, $h(\Theta)$, are defined in the same subroutine, and all can be easily modified to suit different goals. Material coefficients and the initial penalty ε are entered as input. All computations were performed on an IBM RISC/6000 550 in single precision under the AIX operating system.

7.1. Validation of stress update and tangent

To ensure that the stress update and tangent stiffness were properly implemented into the existing code, numerical tests were performed. An extension of the Mooney–Rivlin model was used for the tests and examples:

$$\tilde{W}(\tilde{I}_1, \tilde{I}_2, \tilde{I}_4) = C_1(\tilde{I}_1 - 3) + C_2(\tilde{I}_2 - 3) + C_3(\exp(\tilde{I}_4 - 1) - \tilde{I}_4)\,. \tag{7.1}$$

This form has exponential behavior in the fiber direction, one of the characteristics seen in most soft tissues.

The stress update was validated by comparing the results of one-element tests for uniaxial, strip biaxial and equibiaxial tests to the theoretical solutions for homogeneous deformation. The same material constants were used for all three analyses ($C_1 = 10.0$, $C_2 = 10.0$, $C_4 = 100.0$, $\varepsilon = 10\,000.0$). Fig. 2 illustrates the excellent agreement between the theoretical and finite element solutions.

The convergence behavior of the finite element method for nonlinear problems is controlled by the tangent stiffness in (6.18). If the correct tangent stiffness is implemented, an asymptotically quadratic decrease in the norm of the finite element residual of the right-hand side of (6.18) should be observed when using a full Newton method to solve the system of nonlinear equations.

To assess the convergence behavior, the previous one-element examples were run with large step sizes. For the uniaxial, strip biaxial and equibiaxial problems, the elements were stretched to 75% of their initial length in three equal steps of 25% each. Full Newton iterations were performed at each step. The norm of the residual was plotted as a function of iteration number for each load step. These results are illustrated for the equibiaxial case (Fig. 3). In all cases, asymptotically quadratic decreases in the residual were noted with increasing iteration number.

7.2. A highly constrained problem

Often in biomechanical systems, highly deformable soft tissue structures are interposed between two relatively rigid surfaces. Classic examples of this are the intervertebral discs of the spine and the menisci of the knee. These types of problems are often encountered in engineering problems as well, such as sealing gaps with O-rings. Here, the problem of a cylindrical annulus bonded between two perfectly rigid plates is analyzed (Fig. 4). Because of symmetry, only 1/4 of the total geometry was modeled. Further, to limit the size of the problem, it was modeled as a plane strain configuration – thus the mesh is only one element deep. Applied displacements were used to deform the mesh to 40% axial compression. The sides of the mesh bulge out and eventually contact the plates on the top and bottom. The contact was modeled with a standard penalty method.

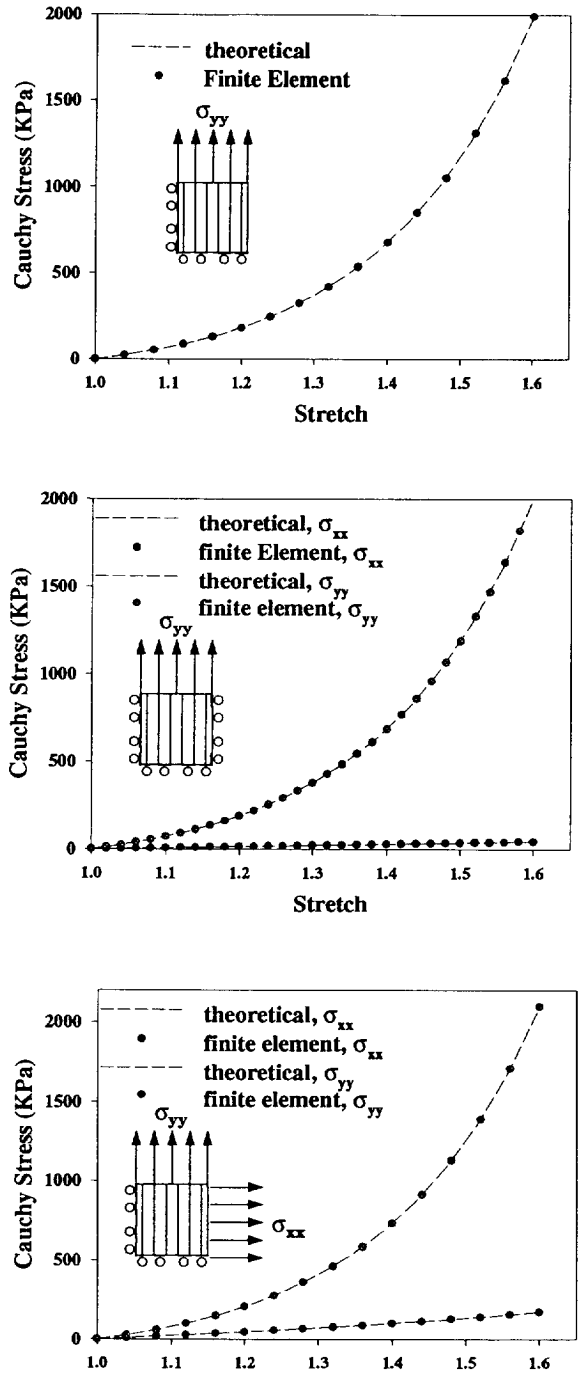

Fig. 2. Comparison of finite element results to theoretical answer for uniaxial, strip biaxial, and equibiaxial extension.

The analysis was run two ways: as an isotropic Mooney–Rivlin material and as a transversely isotropic material represented by (7.1). In the latter case the preferred direction was aligned with the horizontal axis (x direction). The augmented Lagrangian procedure was used to enforce incompressibility. The effect of the incompressibility constraint is evident from examination of Fig. 5, where the solution is computed for both a slightly compressible and fully incompressible material with transverse isotropy along the x direction.

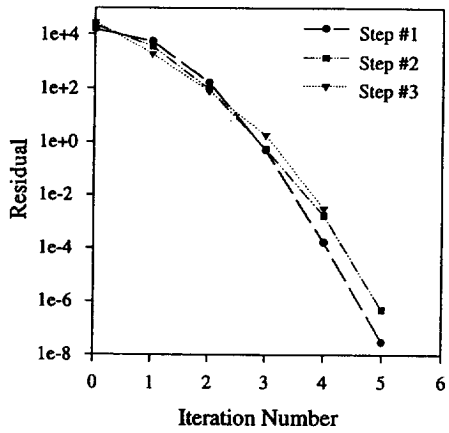

Fig. 3. Plots of the residual (norm of the right-hand side vector in the system of non-linear equations) as a function of iteration number and step for equibiaxial extension.

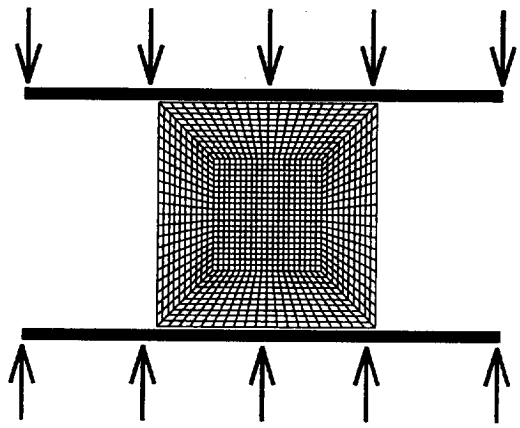

Fig. 4. Undeformed computational mesh of annulus compressed between two plates. Top and bottom of mesh are rigidly bonded to the plates, and the mesh bulges out and contacts the plates as they are pushed together.

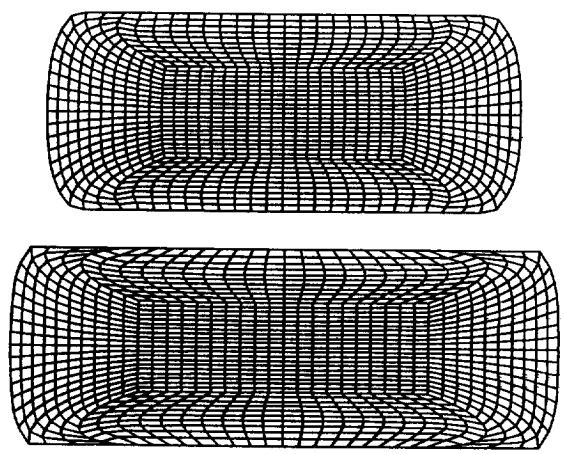

Fig. 5. Deformed mesh at 40% axial compression for both a compressible (top) and incompressible material reinforced in the x direction.

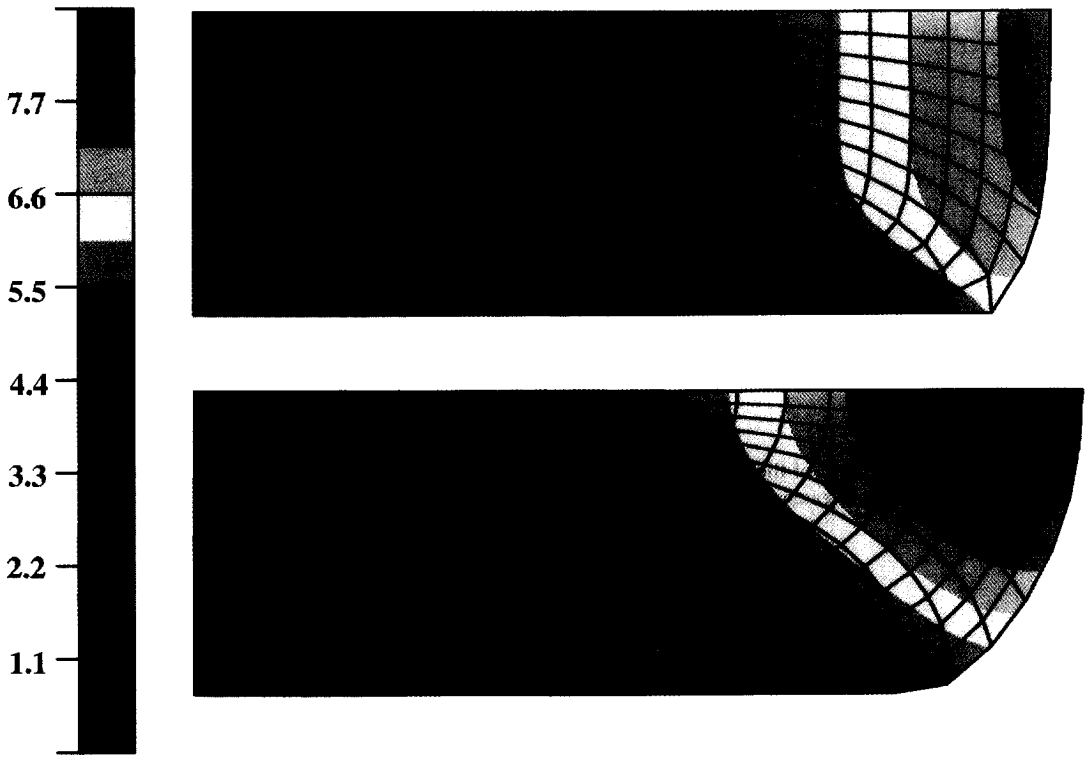

Fig. 6. Fringe plots of the x-displacement for models with preferred direction along x axis (top) and isotropic model; 1/4 symmetry model.

Automatic timestepping and a quasi-Newton solver [21] were used for all solution runs. Fifteen to 30 timesteps were required for the analyses. Five to 10 quasi-Newton iterations were required to achieve convergence at each timestep, followed by 2–5 augmented Lagrangian iterations.

It is easiest to see the differences between the isotropic and transversely isotropic materials by examining the fringes of x-displacement (Fig. 6). First note that the only completely unconstrained direction for the material to deform is in the global x direction. The material with reinforcement in the x direction shows less lateral displacement at the centerline of the annulus (top part of mesh shown). To preserve incompressibility, it undergoes more shearing near the interface with the plate (bottom right part of mesh shown). Looking at the isotropic material, it undergoes considerably more displacement at the centerline of the annulus, and thus less near the interface with the plate. There is less mesh distortion as a result. Thus, the maximum x displacement is greater for the isotropic material. However, the overall volume of both meshes is the same and equal to that of the original (undeformed) mesh.

Examining the fringe plots of pressure (Fig. 7), the interaction between the incompressibility constraint and the material preferred direction becomes evident. For the case of reinforcement in the x direction, the pressures are much higher. As explained, the x direction is really the only direction that has no constraint by boundary conditions. To satisfy the incompressibility constraint, the material must deform in the x direction, and thus the pressure, which equivalently may be thought of as a reaction to the incompressibility constraint, is much higher in the mesh with the x direction as its symmetry axis.

7.3. Modeling the human medial collateral ligament

We are currently developing a detailed model of the human knee (Fig. 8). This model includes realistic hard and soft tissue geometry/material properties for all the major structures, as well as contact surfaces. We recently used the above described finite element implementation to assess the changes in

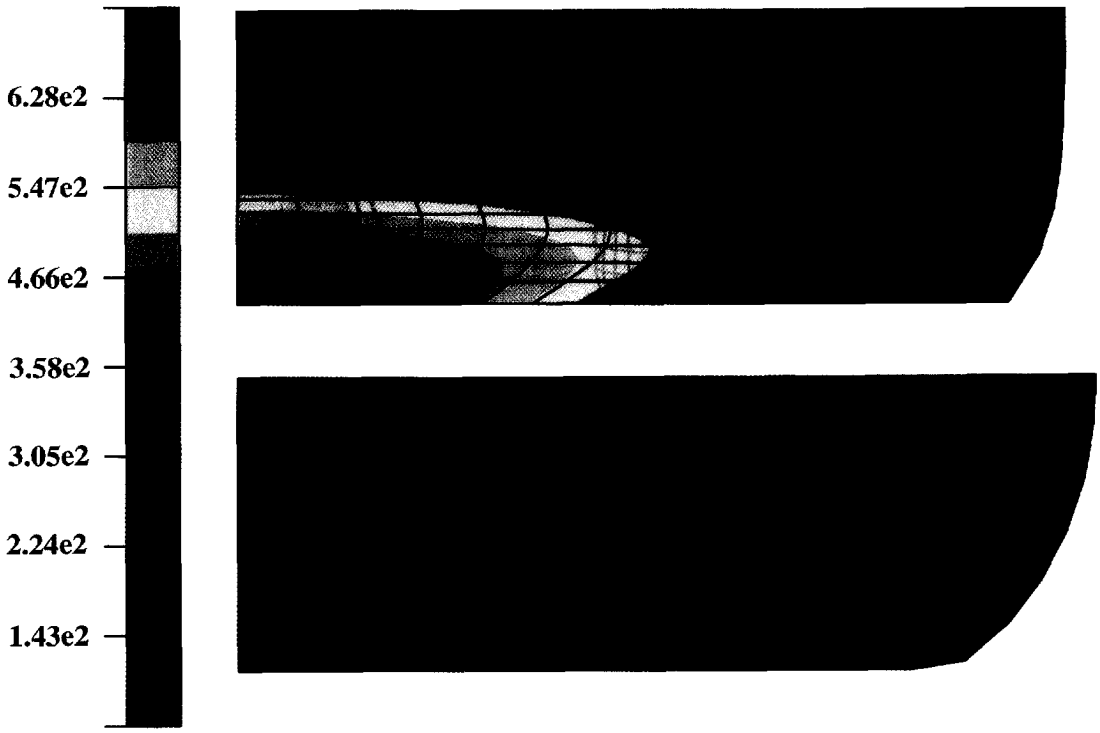

Fig. 7. Fringe plots of pressure for models with preferred direction along x axis (top) and the isotropic case.

the stress state of the medial collateral ligament (MCL) as a function of knee flexion angle. The MCL was modeled using a strain energy specifically designed to capture the behavior of ligamentous structures.

Several observations about the mechanical behavior of collagen fibers were incorporated into the form for F_2. First, collagen does not support a significant compressive load and structures that are composed of mostly collagen will tend to buckle under very small compressive forces. Second, the tensile stress–stretch relation for collagenous tissues such as ligaments and tendons can be well-approximated by an exponential toe region followed by a linear region. These observations led to the following choice for the strain energy of the collagen fiber family:

$$\begin{aligned} \lambda \frac{\partial F_2}{\partial \lambda} &= 0\,, \quad \lambda < 1\,, \\ \lambda \frac{\partial F_2}{\partial \lambda} &= C_3(\exp(C_4(\lambda - 1)) - 1)\,, \quad \lambda < \lambda^*\,, \\ \lambda \frac{\partial F_2}{\partial \lambda} &= C_5\lambda + C_6\,, \quad \lambda \geqslant \lambda^*\,. \end{aligned} \tag{7.2}$$

Here, λ^* is the stretch at which the collagen fibers are straightened, C_3 scales the exponential stresses, C_4 is the rate of uncrimping of the collagen fibers, and C_5 is the modulus of the straightened collagen. C_6 was determined from the condition that the collagen stress is C^0 continuous at λ^*. The form of F_1 was chosen to yield the simplest dependence of the matrix behavior on the invariants I_1 and I_2, namely the neo-Hookean model:

$$\frac{\partial F_1}{\partial I_1} = C_1\,, \qquad \frac{\partial F_1}{\partial I_2} = 0\,. \tag{7.3}$$

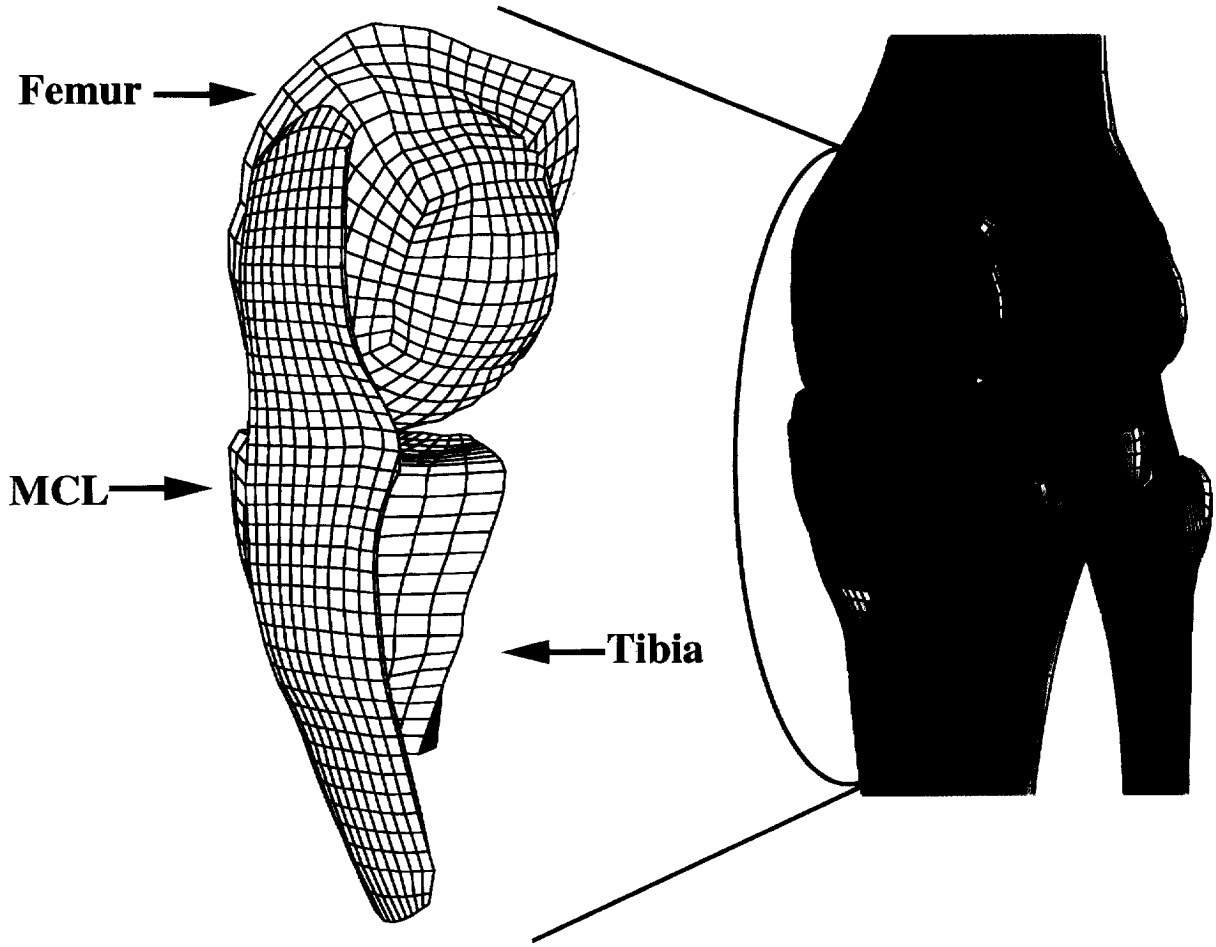

Fig. 8. Detail of a finite element model of the human knee. The constitutive model was used to examine the stresses in the medial collateral ligament (MCL) during knee flexion.

The coefficients were chosen based on material test data:

$$C_1 = 13.85\,\text{MPa}\,, \qquad \lambda^* = 1.03\,,$$
$$C_3 = 2.07\,\text{MPa}\,, \qquad C_4 = 61.44\,, \qquad C_5 = 640.7\,\text{MPa}\,. \tag{7.4}$$

The local fiber direction of the MCL, $\boldsymbol{a}^0$, was specified based on local element geometry to follow the collagen fiber direction between the ligament insertions to bone. Both the femur and tibia were modeled using rigid elements, and frictionless contact was allowed between the MCL and both bones. The attachments of the MCL to the bones were modeled by specifying that the last row of elements in the ligament were part of the same rigid body as the respective bone. An initial tension corresponding to a local fiber stretch of $\lambda = 1.03$ was applied to the structure in its initial configuration [32]. The knee was then flexed to 90 degrees using the rotational degrees of freedom of the rigid femur.

Fig. 9 illustrates the results for the effective stress, both after initial tensioning and following knee flexion. Following flexion, the predicted deformation and stress state correlate well with observations that the anterior edge of the MCL is under the most tension at 90 degrees of knee flexion, while the posterior edge is slack. The buckling of the structure at the posterior aspect also corresponds to our observations of cadaveric knees.

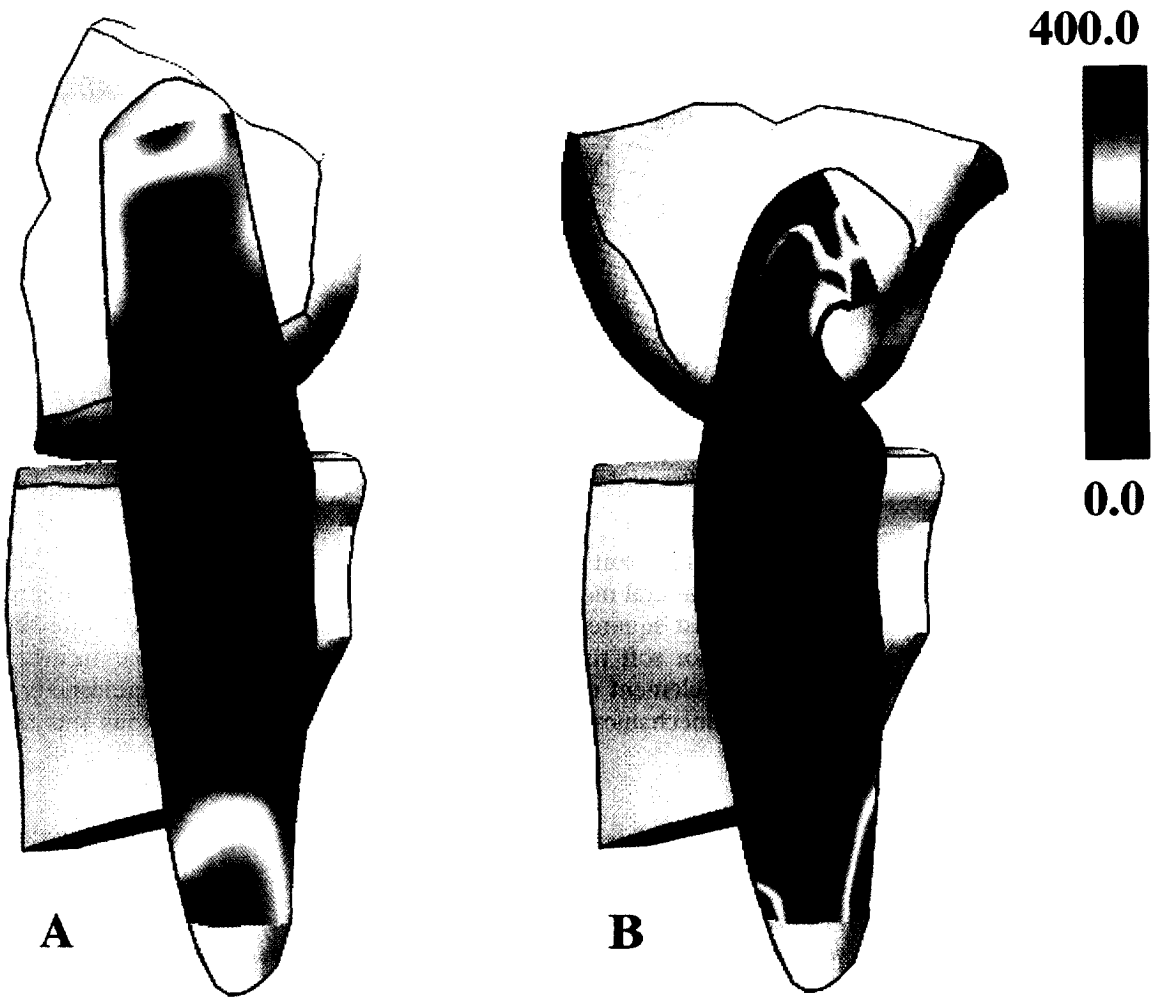

Fig. 9. Effective stress (psi) in the MCL (A) after application of the initial tension, and (B) after the knee was flexed to 90°.

8. Discussion

This paper has presented a constitutive model for incompressible, transversely isotropic, hyperelastic soft tissues and an efficient finite element implementation that allows for fully incompressible material behavior. In addition, original derivations of the elasticity tensors for the above material class were presented.

The interpolation used in this paper may cause a weak mode to occur, which appears as mesh hourglassing in certain situations. In practice, we have only found this to occur for very regular, coarsely zoned meshes. As an example, a minor case of hourglassing was encountered when running a 1/4 symmetry model of an axisymmetric billet compressed between two plates (Fig. 10). It is well known that this mode can be avoided by using a higher-order interpolation for the displacements, pressure and dilation [1, 29]. For example, a quadratic interpolation of displacement, with discontinuous, linear interpolation of pressure and dilation will alleviate this problem, but with an associated increase in computational expense. The design philosophy behind the NIKE3D code has been to use many simple elements with lower order interpolations for the unknowns, rather than higher order elements. This dictated the use of the 8-node brick element with trilinear interpolation for displacements and constant pressure.

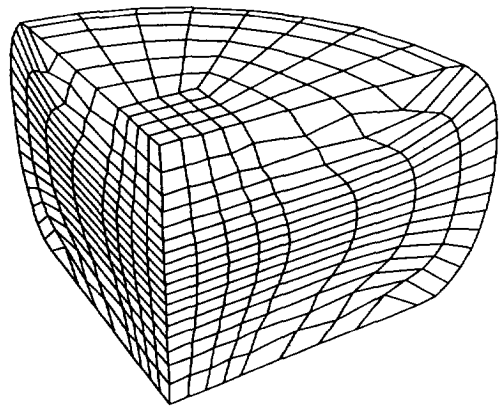

Fig. 10. Illustration of hourglassing for a highly regular mesh of an annulus compressed between two plates; 1/4 symmetry model shown. Note the elements towards the top and bottom of the mesh on the right face.

Along with accurate constitutive models for soft tissues, there is a need for accurate material data as well. We are currently working on experimental methods for determining the material coefficients from test data using constrained non-linear least squares methods. The goal is to obtain an accurate set of material coefficients for each of the major soft tissue structures in the knee. In the near future, the presently described framework for finite element modeling of transversely isotropic hyperelasticity will be used to analyze the details of knee mechanics and the role of each of the ligamentous soft tissue structures.

Acknowledgments

A grant of computer time was provided by the Utah Supercomputing Institute, Salt Lake City, Utah. Partial support for this work was provided under the auspices of the U.S. Department of Energy by the Lawrence Livermore National Laboratory under contract #W-7405-Eng-48.

Appendix A

A.1. Uncoupled stress tensor for a particular $\tilde{W}$

A form similar to (5.1) is used to define the deviatoric strain energy, but instead of the strain energy being a function of the invariants as defined by (3.5) and (3.6), they are functions of their deviatoric counterparts, defined in terms of $\tilde{\boldsymbol{C}}$:

$$\begin{aligned}\tilde{I}_1 &= \operatorname{tr}\tilde{\boldsymbol{C}} = J^{-2/3}\operatorname{tr}\boldsymbol{C}\\ \tilde{I}_2 &= \frac{1}{2}\left((\operatorname{tr}\tilde{\boldsymbol{C}})^2 - \operatorname{tr}\tilde{\boldsymbol{C}}^2\right) = \frac{J^{-4/3}}{2}\left((\operatorname{tr}\boldsymbol{C})^2 - \operatorname{tr}\boldsymbol{C}^2\right)\\ \tilde{I}_4 &= \boldsymbol{a}^0\cdot\tilde{\boldsymbol{C}}\cdot\boldsymbol{a}^0 = J^{-2/3}\boldsymbol{a}^0\cdot\boldsymbol{C}\cdot\boldsymbol{a}^0\,.\end{aligned} \tag{A.1}$$

Clearly, for an incompressible material, these invariants are equivalent to their counterparts defined by (3.5) and (3.6). Now the strain energy in (5.1) is extended to the compressible range and is assumed to take an uncoupled from as defined by (4.4):

$$\begin{aligned}W &= \tilde{W}(\tilde{\boldsymbol{C}}) + U(J)\\ &= \tilde{F}_1(\tilde{I}_1,\tilde{I}_2) + \tilde{F}_2(\tilde{I}_4) + \tilde{F}_3(\tilde{I}_1,\tilde{I}_2,\tilde{I}_4) + U(J)\end{aligned} \tag{A.2}$$

For the strain energy function defined by (5.1),

$$\frac{\partial \tilde{W}}{\partial \tilde{\boldsymbol{C}}} = (\tilde{W}_1 + \tilde{W}_2\tilde{I}_1)\mathbf{1} - \tilde{W}_2\tilde{\boldsymbol{C}} + \tilde{W}_4\boldsymbol{a}^0\otimes\boldsymbol{a}^0\,, \tag{A.3}$$

where $\tilde{W}_a = \partial\tilde{W}/\partial\tilde{I}_a$. Next, one can compute

$$\mathrm{DEV}\left[\frac{\partial \tilde{W}}{\partial \tilde{\boldsymbol{C}}}\right] = (\tilde{W}_1 + \tilde{W}_2\tilde{I}_1)\mathbf{1} - \tilde{W}_2\tilde{\boldsymbol{C}} + \tilde{W}_4\boldsymbol{a}^0\otimes\boldsymbol{a}^0 - \frac{1}{3}(\tilde{W}_1\tilde{I}_1 + 2\tilde{W}_2\tilde{I}_2 + \tilde{W}_4\tilde{I}_4)\tilde{\boldsymbol{C}}^{-1}\,. \tag{A.4}$$

Now the 2nd Piola–Kirchhoff stress is given by (4.5):

$$\boldsymbol{S} = pJ\boldsymbol{C}^{-1} + 2J^{2/3}[(\tilde{W}_1 + \tilde{W}_2\tilde{I}_1)\mathbf{1} - \tilde{W}_2\tilde{\boldsymbol{C}} + \tilde{W}_4\boldsymbol{a}^0\otimes\boldsymbol{a}^0 - \tfrac{1}{3}(\tilde{W}_1\tilde{I}_1 + 2\tilde{W}_2\tilde{I}_2 + \tilde{W}_4\tilde{I}_4)\tilde{\boldsymbol{C}}^{-1}]\,. \tag{A.5}$$

To get the Cauchy stress, the push-forward of (A.3) is

$$\tilde{\boldsymbol{F}}\,\frac{\partial \tilde{W}}{\partial \tilde{\boldsymbol{C}}}\,\tilde{\boldsymbol{F}}^{\mathrm{T}} = (\tilde{W}_1 + \tilde{W}_2\tilde{I}_1)\tilde{\boldsymbol{B}} - \tilde{W}_2\tilde{\boldsymbol{B}}^2 + \tilde{W}_4\tilde{I}_4\boldsymbol{a}\otimes\boldsymbol{a} \tag{A.6}$$

The Cauchy stress then follows from (4.7):

$$\boldsymbol{\sigma} = p\mathbf{1} + \frac{2}{J}[(\tilde{W}_1 + \tilde{W}_2\tilde{I}_1)\tilde{\boldsymbol{B}} - \tilde{W}_2\tilde{\boldsymbol{B}}^2 + \tilde{W}_4\tilde{I}_4\boldsymbol{a}\otimes\boldsymbol{a} - \frac{1}{3}(\tilde{W}_1\tilde{I}_1 + 2\tilde{W}_2\tilde{I}_2 + \tilde{W}_4\tilde{I}_4)\mathbf{1}]\,. \tag{A.7}$$

A.2. Uncoupled elasticity tensor for a particular W

Now the form of $\mathbf{C}$ and $\mathbf{c}$ for the strain energy function defined by (4.4) must be determined. Examining the form of (4.9), it is seen that everything required has already been computed except $\tilde{\mathbf{C}}$. Looking at (4.10), the second derivative of $\tilde{W}$ is required. Working from (3.20) and omitting the vanishing 2nd derivatives of W, and replacing the invariants and the right Cauchy–Green deformation with the corresponding deviatoric quantities,

$$\begin{aligned}\frac{\partial^2 \tilde{W}}{\partial \tilde{\boldsymbol{C}}\,\partial \tilde{\boldsymbol{C}}} = {} & (\tilde{W}_{11} + 2\tilde{W}_{12}\tilde{I}_1 + \tilde{W}_2 + \tilde{W}_{22}\tilde{I}_1^2)\mathbf{1}\otimes\mathbf{1} \\ & - (\tilde{W}_{12} + \tilde{W}_{22}\tilde{I}_1)(\mathbf{1}\otimes\tilde{\boldsymbol{C}} + \tilde{\boldsymbol{C}}\otimes\mathbf{1}) \\ & + \tilde{W}_{22}(\tilde{\boldsymbol{C}}\otimes\tilde{\boldsymbol{C}}) - \tilde{W}_2\boldsymbol{I} \\ & + (\tilde{W}_{14} + \tilde{W}_{24}\tilde{I}_1)(\mathbf{1}\otimes\boldsymbol{a}^0\otimes\boldsymbol{a}^0 + \boldsymbol{a}^0\otimes\boldsymbol{a}^0\otimes\mathbf{1}) \\ & - \tilde{W}_{24}(\tilde{\boldsymbol{C}}\otimes\boldsymbol{a}^0\otimes\boldsymbol{a}^0 + \boldsymbol{a}^0\otimes\boldsymbol{a}^0\otimes\tilde{\boldsymbol{C}}) + \tilde{W}_{44}(\boldsymbol{a}^0\otimes\boldsymbol{a}^0\otimes\boldsymbol{a}^0\otimes\boldsymbol{a}^0)\,,\end{aligned} \tag{A.8}$$

$$\begin{aligned}\frac{\partial^2 \tilde{W}}{\partial \tilde{\boldsymbol{C}}\,\partial \tilde{\boldsymbol{C}}} : \tilde{\boldsymbol{C}} = {} & (\tilde{W}_{11}\tilde{I}_1 + 2\tilde{W}_{12}\tilde{I}_1^2 - \tilde{W}_{12}\tilde{I}_1 + W_2 I_1 \\ & + \tilde{W}_{22}\tilde{I}_1^2 + \tilde{W}_{22}\tilde{I}_1^3 + \tilde{W}_{14}\tilde{I}_4 + \tilde{W}_{24}\tilde{I}_1\tilde{I}_4)\mathbf{1} \\ & - (\tilde{W}_{12} + \tilde{W}_{22}\tilde{I}_1 - \tilde{W}_{22}\tilde{I}_1^2 + 2\tilde{W}_{22}\tilde{I}_2 + \tilde{W}_2 + \tilde{W}_{24}\tilde{I}_4)\tilde{\boldsymbol{C}} \\ & + (\tilde{W}_{14}\tilde{I}_1 + 2\tilde{W}_{24}\tilde{I}_2 + \tilde{W}_{44}\tilde{I}_4)\boldsymbol{a}^0\otimes\boldsymbol{a}^0\,,\end{aligned} \tag{A.9}$$

and

$$\begin{aligned}\tilde{\boldsymbol{C}} : \frac{\partial^2 \tilde{W}}{\partial \tilde{\boldsymbol{C}}\,\partial \tilde{\boldsymbol{C}}} : \tilde{\boldsymbol{C}} = {} & (\tilde{W}_{11}\tilde{I}_1 + 2\tilde{W}_{12}\tilde{I}_1^2 - \tilde{W}_{12}\tilde{I}_1 + \tilde{W}_2\tilde{I}_1 \\ & + \tilde{W}_{22}\tilde{I}_1^2 + \tilde{W}_{22}\tilde{I}_1^3 + \tilde{W}_{14}\tilde{I}_4 + \tilde{W}_{24}\tilde{I}_1\tilde{I}_4)\tilde{I}_1 \\ & - (\tilde{W}_{12} + \tilde{W}_{22}\tilde{I}_1 - \tilde{W}_{22}\tilde{I}_1^2 + 2\tilde{W}_{22}\tilde{I}_2 \\ & + \tilde{W}_2 + \tilde{W}_{24}\tilde{I}_4)(\tilde{I}_1^2 - 2\tilde{I}_2) \\ & + (\tilde{W}_{14}\tilde{I}_1 + 2\tilde{W}_{24}\tilde{I}_2 + \tilde{W}_{44}\tilde{I}_4)\tilde{I}_4\,.\end{aligned} \tag{A.10}$$

Now $\mathbf{C}$ follows directly from (4.10) and (4.9). The spatial elasticity tensor, $\mathbf{c}$, as defined by (4.11), follows by the push-forward of $\tilde{\mathbf{C}}$ by $\tilde{F}$.

References

[1] I. Babuska, The finite element method with Lagrangian multipliers, Numer. Math. 20 (1973) 179–192.
[2] K-J. Bathe, Finite Element Procedures in Engineering Analysis (Prentice-Hall, Englewood Cliffs, NJ, 1982).
[3] C.J. Choung and Y.C. Fung, Residual stress in arteries, in: Frontiers in Biomechanics (Springer-Verlag, New York, 1986) 117–179.
[4] P.J. Flory, Thermodynamic relations for high elastic materials, Trans. Faraday Soc. 57 (1961) 829–838.
[5] Y.C. Fung, Foundations of Solid Mechanics (Prentice-Hall, Englewood Cliffs, NJ, 1965).
[6] Y.C. Fung, Elasticity of soft tissues in simple elongation, Am. J. Physiol. 213 (1967) 1532–1544.
[7] Y.C. Fung, Biomechanics: Mechanical Properties of Living Tissues (Springer-Verlag, New York, 1981).
[8] S. Govindjee and J.C. Simo, Mullins' effect and the strain amplitude dependence of the storage modulus, Int. J. Solids Struct. 29 (1992) 1737–1751.
[9] A.E. Green, Large Elastic Deformations (Clarendon Press, Oxford, UK, 1970).
[10] J.M. Guccione, A.D. McCulloch and L.K. Waldman, Passive material properties of intact ventricular myocarcium determined from a cylindrical model, ASME J. Biomech. Engrg. 113 (1991) 42–55.
[11] A. Horowitz, I. Sheinman and Y. Lanir, Nonlinear incompressible finite element for simulating loading of cardiac tissue—Part II: Three-dimensional formulation for thick ventricular wall segments, ASME J. Biomech. Engrg. 110 (1988) 62–68.
[12] T.J.R. Hughes, Generalization of selective integration procedures to anisotropic and nonlinear media, Int. J. Numer. Methods Engrg. 15 (1980) 1413–1418.
[13] J.D. Humphrey, R.K. Strumph and F.C.P. Yin, Determination of a constitutive relation for passive myocardium, I. A new functional form, ASME J. Biomech. Engrg. 112 (1990) 333–339.
[14] J.D. Humphrey and F.C.P. Yin, On constitutive relations and finite deformations of passive cardiac tissue: I. A pseudostrain-energy approach, ASME J. Biomech. Engrg. 109 (1987) 298–304.
[15] J.M. Huyghe, D.H. van Campen, T. Arts and R.M. Heethaar, The constitutive behavior of passive heart muscle tissue: A quasi-linear viscoelastic formulation, J. Biomech. 24 (1991) 841–849.
[16] E. Hvidberg, Investigations into the effect of mechanical pressure on the water content of isolated skin, Acta Pharmac. (Kobenhavn) 16 (1960) 245–259.
[17] S.W. Key, A variational principle for incompressible and nearly-incompressible anisotropic elasticity, Int. J. Solids Struct. 5 (1969) 951–964.
[18] Y. Lanir, Constitutive equations for fibrous connective tissues, J. Biomech. 16 (1983) 1–12.
[19] B.N. Maker, R.M. Ferencz and J.O. Hallquist, Nike3d: A nonlinear, implicit, three-dimensional finite element code for solid and structural mechanics, Lawrence Livermore National Laboratory Technical Report, UCRL-MA-105268, 1990.
[20] J.E. Marsden and T.J.R. Hughes, The Mathematical Foundations of Elasticity (Prentice-Hall, Englewood Cliffs, NJ, 1983).
[21] H. Matthies and G. Strang, The solution of nonlinear finite element equations, Int. J. Numer. Methods Engrg. 14 (1979) 1613–1626.
[22] M. Mooney, A theory of large elastic deformation, J. Appl. Phys. 11 (1940) 582–592.
[23] J.T. Oden and N. Kikuchi, Finite element methods for constrained problems in elasticity, Int. J. Numer. Methods Engrg. 18 (1982) 701–725.
[24] J.C. Simo, On a fully three-dimensional finite-strain viscoelastic damage model: Formulation and computational aspects, Comput. Methods Appl. Mech. Engrg. 60 (1987) 153–173.
[25] J.C. Simo and R.L. Taylor, Quasi-incompressible finite elasticity in principal stretches: Continuum basis and numerical algorithms, Comput. Methods Appl. Mech. Engrg. 85 (1991) 273–310.
[26] J.C. Simo, R.L. Taylor and K.S. Pister, Variational and projection methods for the volume constraint in finite deformation elastoplasticity, Comput. Methods Appl. Mech. Engrg. 51 (1985) 177–208.
[27] G.F. Smith and R.S. Rivlin, Integrity bases for vectors. The crystal classes, Arch. Rat. Mech. Anal. 15 (1994) 169–221.
[28] A.J.M. Spencer, Continuum Theory of the Mechanics of Fibre-Reinforced Composites (Springer-Verlag, New York, 1984).
[29] T. Sussman and K-J. Bathe, A finite element formulation for nonlinear incompressible elastic and inelastic analysis, Comput. Struct. 26 (1987) 357–409.
[30] K. Washizu, Variational Methods in Elasticity and Plasticity (Pergamon, Oxford, 1974).
[31] J.A. Weiss, A constitutive model and finite element representation for transversely isotropic soft tissues, Ph.D. Thesis, Department of Bioengineering, The University of Utah, 1994.
[32] J.A. Weiss, B.N. Maker and D.A. Schauer, Treatment of initial stress in hyperelastic finite element models of soft tissues, Proc. ASME Summer Bioengineering Conference, BED-29: 105–106, 1995.
[33] S.L-Y. Woo and J.A. Buckwalter, Injury and Repair of the Musculoskeletal Soft Tissues, American Academy of Orthopaedic Surgeons, Park Ridge, Illinois, 1988.
[34] F.C.P. Yin, R.K. Strumph, P.H. Chew and S.L. Zeger, Quantification of the mechanical properties of noncontracting canine myocardium under simultaneous biaxial loading, J. Biomech. 20 (1987) 577–589.